1998MNRAS.298..131B

Mon. Not. R. Astron. Soc. **298,** 131–138 (1998)

The 10-μm profile of molecular-cloud and diffuse ISM silicate dust

J. E. Bowey,[1] A. J. Adamson[1] and D. C. B. Whittet[2]

[1] *University of Central Lancashire, Centre for Astrophysics, Preston PR1 2HE*

[2] *Department of Physics, Applied Physics and Astronomy, Rensselaer Polytechnic Institute, Troy, NY 12180, USA*

Accepted 1998 March 2. Received 1998 February 18; in original form 1996 August 16

ABSTRACT

High signal-to-noise ratio spectra are presented of the 10-μm silicate absorption feature in lines of sight towards Elias 16 and 18 in the Taurus dark cloud, and towards the heavily reddened supergiant Cyg OB2 no. 12. The observations are fitted with laboratory and astronomical spectra to produce intrinsic absorption profiles. These features, which represent molecular-cloud and diffuse ISM dust respectively, are better fitted with emissivity spectra of the Trapezium and μ Cephei than they are with those of laboratory, terrestrial, or other observations of circumstellar silicates. The difference in width between the silicate band in the two environments can be almost entirely ascribed to a broad excess absorption in the long-wavelength wing of the profiles, which is much stronger in the molecular-cloud lines of sight, and possibly reflects grain growth in the denser environment. Limits are placed on the strength of fine spectral structure; if there is a crystalline silicate component in these spectra, it is most likely to be serpentine. Column-density upper limits for methanol and the photolysis product hexamethylenetetramine (HMT) are less than a few per cent of those of water ice and silicates.

Key words: ISM: clouds – dust, extinction – ISM: molecules – infrared: ISM: lines and bands.

1 INTRODUCTION

Silicates are ubiquitous in virtually all astronomical particulate material. They are present in meteorites and interplanetary dust particles (IDPs), and their presence in comets and the ISM is revealed by a broad spectral feature centred close to 9.7 μm, consistent with Si–O stretching vibrations. This band has been detected in a wide range of Galactic environments. Interstellar silicate grains mainly originate in the atmospheres and outflows of evolved post-main-sequence stars having elemental abundances similar to those of the Sun. As the temperature in the outflowing wind drops to ~1000 K, iron and $MgSiO_3$ solids condense. FeO and hydrous silicates such as serpentine are expected to form below 500 K. Subsequently, the SiO clusters may absorb Mg, water and iron to form minerals similar to terrestrial olivines and pyroxenes. The first silicate (emission) bands observed beyond the Solar system were found to be due to circumstellar grains grown in non-equilibrium conditions and hence deficient in oxygen (reviewed by Jäger et al. 1994). Some interplanetary dust particles may be pre-solar; their spectra are again consistent with olivines, layer-lattice silicates and pyroxenes (Sandford & Walker 1985).

Laboratory analogues of interstellar silicates (e.g. Day & Donn 1978; Stephens & Russell 1979) have produced spectra which broadly resemble the 10-μm emission feature of, for example, the Orion Trapezium region, but in general these spectra do not match the observations particularly well. For example, Roche & Aitken (1985) noted very poor fits to the silicate absorption feature in lines of sight toward the Galactic Centre.

A variety of effects can alter the shape of the silicate feature in astronomical sources. Increasing particle size broadens the feature and shifts it to a longer wavelength (Hanner, Lynch & Russell 1994b). Dorschner et al. (1988) showed that the spectra of bronzite grains are size-dependent for grain radii $\geq$0.3 μm: increasing the mean particle radius to 1.0 μm shifts the peak from 9.5 to 9.8 μm and widens the band from 2.5 to 2.8 μm FWHM. Differences in chemical composition can alter the entire feature: Blanco et al. (1993) found peak wavelengths between 9.6 and 10.0 μm, and FWHM between 1.9 and 2.3 μm in amorphous samples of varying composition. Simpson (1991) suggested that variations on the short-wavelength side of the 9.7-μm band must reflect differences in chemical composition, but both Gürtler et al. (1993) and Jäger et al. (1994) found that the chemical composition of pyroxene melts affects the band shape much less than the degree of crystallinity. There is also evidence from both cometary spectra and interplanetary dust particles that initially amorphous silicates become more crystalline with time and thermal processing, producing structure in the 10-μm feature (e.g. Bregman et al. 1987; Campins & Ryan 1989; Sandford 1989; Hanner, Brooke & Tokunaga 1994a).

The most abundant pyroxene in chondritic meteorites, IDPs and cometary dust has bronzite stoichiometry ($[Mg,Fe]SiO_3$). In amorphous form it has the broadest feature seen in amorphous silicates (Dorschner et al. 1988), although it is still narrower than the feature produced by dust in molecular clouds. The spectra of dust shells

© 1998 RAS

© Royal Astronomical Society • Provided by the NASA Astrophysics Data System

1998MNRAS.298..131B

around mass-losing O-rich giants and supergiants are better fitted by the narrower feature of olivine-like silicates, which peaks at ~9.9 μm. In the molecular clouds, it is possible that mantling with H_2O ice affects the silicate band both through the effect of the mantles' optical properties, and by the presence of additional spectral features in the 15-μm region.

To provide a constraint on the silicate mineralogy that is independent of the properties of the continuum source, and not affected by underlying silicate emission, this paper presents observations of silicate features in pure absorption. The properties of cold molecular-cloud dust are observed in the lines of sight to three sources from the Elias 2-μm survey of the Taurus dark cloud: Elias 16 is a background field star which samples quiescent dust in a region of the cloud remote from any embedded source, while Elias 18 is an embedded object which allows us to investigate the effect of heating on dust in its vicinity. A second field star, Elias 13, was also observed (but with lower signal-to-noise ratio due to its relative faintness). The diffuse ISM is represented by the heavily reddened supergiant Cygnus OB2 no. 12 (see Adamson, Whittet & Duley 1990 and Whittet et al. 1997 for reviews of this line of sight and the degree to which it represents the diffuse ISM).

2 OBSERVATIONS AND REDUCTION

2.1 Observations

8–13 μm spectroscopy was carried out using CGS3 at the UK Infrared Telescope on Mauna Kea, Hawaii on 1993 November 7 and 8 (UT). Weather conditions were excellent. The spectrometer was used in low-resolution mode, producing spectra centred at 10.5 μm, wavelength-calibrated by a krypton arc lamp. The aperture was 5.5 arcsec, and the chop 5 Hz (through 20 arcsec in a direction tailored to the object). Standard stars used for cancellation of telluric absorption and for flux calibration are listed in Table 1. Ideally, such standards have flux spectra approximating a Planck function; this is true for Sirius and η Cyg, but α Tau has anomalous absorption in this part of its spectrum. Observations ratioed against α Tau were corrected by cross-calibration against another standard.

2.2 Reduction to flux spectra

CGS3 achieves complete spectral sampling by interleaving two spectra shifted by a small wavelength increment (referred to as a 'pair'). A number of pairs were obtained for each object. Transparency variations between the two spectra in a pair can produce a ripple with a period of two pixels; where present, this was removed using the FIGARO IRFLAT routine. The resulting flux spectra are shown in Fig. 1. To estimate the degree of scatter due to variations in transparency *between* pairs, the errors were derived in two ways: first from the scatter between pairs, and secondly from the scatter after normalizing all pairs to the same mean value. Over most of the spectrum the resulting error bars were consistent to within 20 per cent, but at the short-wavelength end (7.8–9.0 μm) errors in the unnormalized spectrum were significantly higher. To allow for this in the fitting process, the mean normalized spectrum, weighted with the *unnormalized* errors, was fitted.

3 FITTING THE SILICATE FEATURE

3.1 Taurus field stars and Cyg OB2 no. 12

Silicate spectra of the field objects were analysed relative to a continuum derived by fitting existing broad-band photometry.

Table 1. Standard stars

Name	BS	T_{eff}
Sirius	2491	9200
η Cyg	7949	4790
α Tau	1457	3980

Infrared photometric data catalogued by Gezari et al. (1993) were fitted with a reddened Planck function:

$$F_\nu = c_1 B_\nu(T) e^{-\tau_{\rm cont}(\lambda)},$$

where $B_\nu(T)$ is the Planck function, c_1 is a normalization constant, and $\tau_{\rm cont}(\lambda)$ is the continuum extinction optical depth:

$$\tau_{\rm cont}(\lambda) = \tau_{\rm cont}(1.65\,\mu{\rm m})\left(\frac{\lambda}{1.65}\right)^{-1.8}.$$

The exponent (−1.8) is the mean value adopted by Martin & Whittet (1990), and $\tau_{\rm cont}$ (1.65 μm) – the extinction optical depth in the H band – is a fitted parameter. Photometric points between 8.5 and 12.0 μm were excluded, and where no broad-band mid-infrared points were available, the photometry was supplemented with fluxes measured from our spectra (accurate to ~10 per cent). Optimum values of T, c_1 and $\tau_{\rm cont}$ (1.65 μm) were determined using the downhill simplex method (Press et al. 1992). The results are shown in Table 2. Although photometry for Elias 13 is sparse, and its fit is not well constrained, temperatures fitted to Elias 13 and 16 are close to the colour temperatures observed by Elias (1978); these spectra are consistent with late-type photospheres, unaffected by the presence of heated local dust.

The fitted temperature of Cyg OB2 no. 12 is consistent with that determined by Rieke (1974), and the fitted H-band optical depth corresponds to a visual extinction of 10.2 mag, close to the centre of the standard range of 9.9 to 10.4 mag (Humphreys 1978). This suggests that continuous emission from the stellar wind is not a major contributor to the mid-infrared continuum emission. The hydrogen 7–6 line seen at 12.3 μm in this spectrum is the only emission line detected; it was excluded when fitting the silicate feature.

These continua were used as the basis for the band-fitting described in the next section. Since it is likely that these are pure absorption features, the function fitted was

$$F_\nu = c_2 B_\nu(T) e^{-\tau_{\rm cont}(\lambda)} e^{-\tau_0 \epsilon(\lambda)},$$

where $\epsilon(\lambda)$ is the silicate emissivity used to model the feature optical depth, and τ_0 is the peak optical depth of the feature. c_2 and τ_0 were fitted, while T and $\tau_{\rm cont}$ (1.65 μm) were held constant at the values determined in fitting the photometry.

3.2 Elias 18

The continuum spectrum of Elias 18 is not well represented by a single reddened blackbody, implying the presence of heated dust local to this source; the possible presence of CO_2 (Chiar et al. 1995) and detection of the 'XCN' carrier (Tegler et al. 1995) in this line of sight also show that the grains are more processed than those towards Elias 16. The 8–13 μm spectrum was therefore fitted using a three-component model to simulate the presence of a hot photosphere, hot optically thick dust emission, and a cooler optically thin region (all subjected to foreground extinction). The

© Royal Astronomical Society • Provided by the NASA Astrophysics Data System

1998MNRAS.298..131B

Table 2. Fitted temperature (T) and H-band continuum optical depth ($\tau_{1.65}$) for field stars.

Object	T/K	$\tau_{1.65}$	Photometry Reference
Cyg OB2 no.12	11000	1.35	Abbott et al. 1984; Rieke 1974; Persi & Ferrari-Toniolo 1982
Taurus-Elias 13	4400	2.0	Elias 1978; Tamura & Sato 1989
Taurus-Elias 16*	4600	2.3	Elias 1978

*8-and 13-μm points taken from our own observations between 7.8 and 8-μm and 12.3 and 13-μm. These fluxes were then raised to the level of the rest of the photometry.

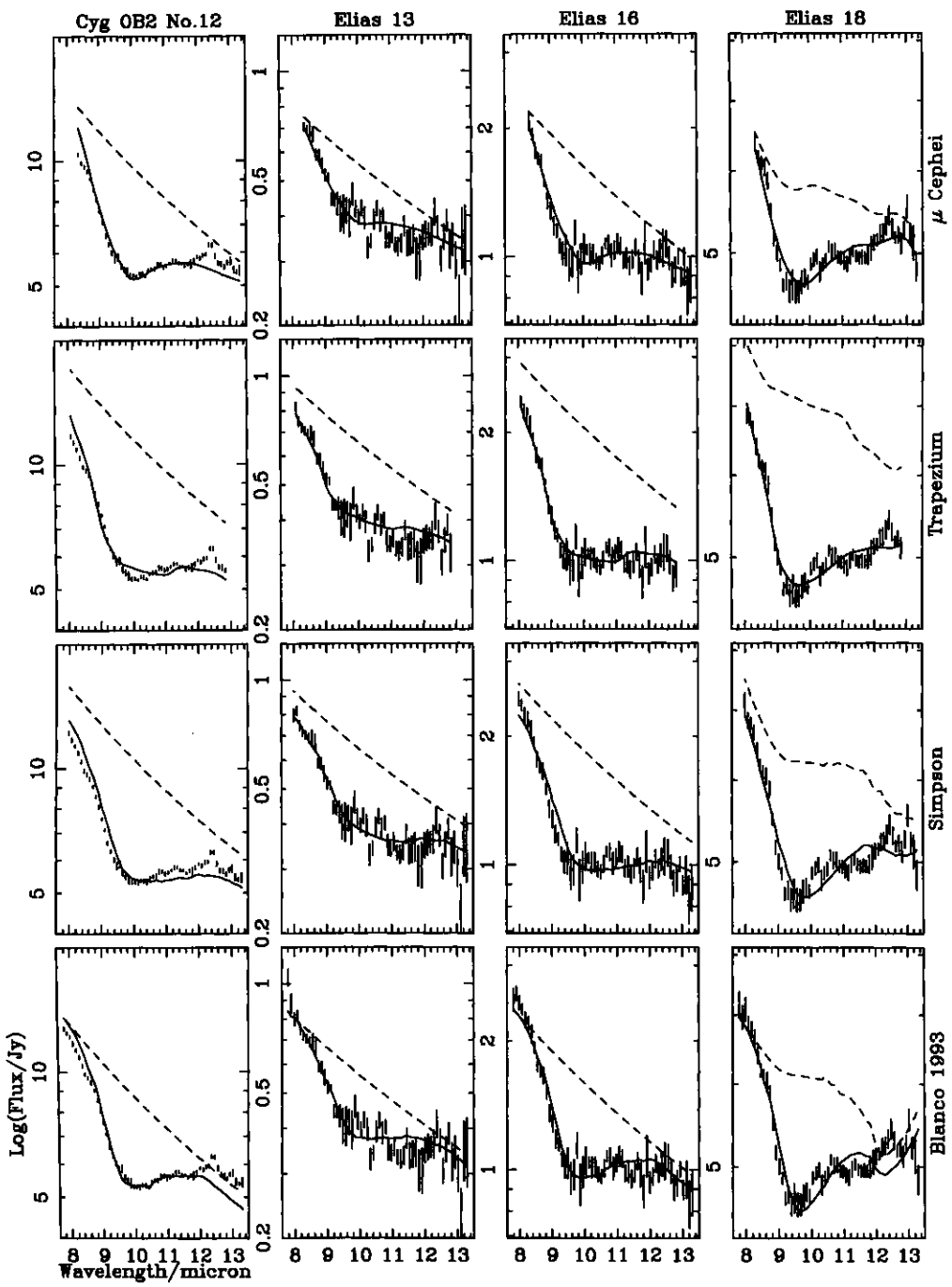

Figure 1. Flux spectra, with modelled fluxes as calculated in Section 3.

© 1998 I

© Royal Astronomical Society • Provided by the NASA Astrophysics Data System

1998MNRAS.298..131B

Table 3. Astronomical and laboratory emissivity spectra fitted to observed 9.7-μm silicate features.

Source	Trapezium		μ Cephei		Simpson		Blanco	
	τ_0*	χ_ν^2	τ_0	χ_ν^2	τ_0†	χ_ν^2	τ_0‡	χ_ν^2
Cyg OB2 no.12	0.77	34	0.64	31	0.68 (1)	45	0.53 (d)	38
Taurus-Elias 13	0.52	1.9	0.38	1.8	0.52 (2)	1.5	0.42 (o)	2
Taurus-Elias 16	0.75	1.1	0.53	1.4	0.66 (1)	2.3	0.55 (d)	1.6
Taurus-Elias 18	0.42	2.0	0.21	2.8	0.30 (1)	4.6	0.30 (d)	4.6

* τ_0 is the optical depth of the fitted feature. Inferred depths of the *observed* features are given in Table 5.

† Numbers in brackets refer to emissivity groups given in Table 4.

‡ Letters in brackets refer to diopside (d) and synthetic olivine (o).

Table 4. Characteristics of Simpson's circumstellar emissivity groups.

Group	Wavelength of Peak Emissivity	FWHM(μm)	Characteristics
1	9.8	3.0	narrow
2	9.7	3.3	broader on long wavelength side
3	10.0	2.9	as for Group 2
4	9.8	3.6	broader than Group 2, partially filling 14μm-16μm region
5	10.0	3.6	as for Group 4

function fitted was

$$F_\nu = (F_{\rm source})e^{-[\tau_0\epsilon(\lambda)+\tau_{\rm cont}(\lambda)]},$$

where

$$F_{\rm source} = [a_0 B_\nu(T_0) + a_1 B_\nu(T_1) + a_2\epsilon_\lambda B_\nu(T_2)],$$

with photospheric (T_0), optically thick (T_1) and optically thin (T_2) temperatures fixed at 15 400, 1000 and 250 k respectively. a_0, a_1, a_2 are free parameters, and $\tau_{\rm cont}$ (1.65 μm) was fixed at 2.7.

4 THE SILICATE SPECTRUM

The observed spectra were fitted with interstellar and circumstellar silicate emissivities, and with laboratory spectra of artificial silicates and terrestrial minerals. It is shown later that the fine structure expected from crystalline silicates is absent from the spectra. Since the best available spectrum of a comet – that of comet Halley – shows fine structure due to crystalline silicates (Bregman et al. 1987; Campins & Ryan 1989), no comparison with cometary spectra was attempted.

4.1 The Trapezium and μ Cephei emissivities

Circumstellar silicate emission observed in μ Cephei (Russell, Soifer & Forrest 1975) has often been used to represent interstellar silicate features in the diffuse ISM (e.g. Roche & Aitken 1984, 1985). Molecular cloud dust is commonly considered to be better represented by the spectrum of the Orion Trapezium (observed by Forrest, Gillett & Stein 1975; see Roche & Aitken 1984 and Whittet et al. 1988). For compatibility with previous work, we fit using smoothed versions of the Trapezium and μ Cephei emissivities from the above references.[1] The emissivity functions $\epsilon(\lambda)$ normally adopted assume a single temperature for the emitting grains. An emission temperature of 250 K was adopted for both; Trapezium fits with a lower temperature produced significantly worse χ_ν^2 in all cases. Fit parameters are given in Table 3, and the fits are shown in the first two rows of Fig. 1. Cyg OB2 no. 12 is best fitted by μ Cephei. Elias 16 and 18 are better fitted by the Trapezium, despite the probable difference between heated dust in the Trapezium and quiescent, ice-mantled dust in the Taurus cloud. In this and other cases, the Elias 18 spectrum was better fitted with the inclusion of a proportion of optically thin silicate emission, evident in the 'continuum' plotted in Fig. 1. This produces ~15 per cent of the flux at 9.7 μm when modelled by the Trapezium emissivity, with the remainder contributed entirely by the hot photosphere; this is consistent with Elias 18's falling mid-infrared spectrum, which suggests that it is a relatively evolved YSO. Formally, the noisy spectrum of Elias 13 is better fitted by Simpson's Group 2 circumstellar emissivity (described in Section 4.2).

4.2 Other circumstellar emissivities

Simpson (1991) extracted high-quality, optically thin 8–23 μm silicate emission spectra from the *IRAS* LRS atlas, and divided them into five groups whose characteristics are described in Table 4. The widths[2] of these features lie between those of the Trapezium (broad) and μ Cephei (narrow). We have compared the average spectrum of each group with the UKIRT spectra, using the fitting method described previously. The best fits are shown in the third row of Fig. 1. Group 1 produces the best fits to Elias 16, 18 and Cyg OB2 no. 12 (Table 3). The feature in Elias 13 appears to be broader on the long-wavelength side, producing a better formal match to Group 2; but the signal-to-noise ratio is poor. In all cases, the peak fitted optical depths are at the same wavelength as those derived using the Trapezium and μ Cephei emissivities.

[1] There has been a recent determination of the Trapezium emissivity (Hanner, Brooke & Tokunaga 1995). The Hanner et al. function has the same shape on the long-wavelength side of the peak, but the short-wavelength wing occurs at longer wavelengths, and consequently the peak is shifted to a wavelength more comparable to that seen in μ Cephei.

[2] We define the width of a feature to be its FWHM, and its value therefore depends on the level of optical depth at the band edges.

© Royal Astronomical Society • Provided by the NASA Astrophysics Data System

1998MNRAS.298..131B

Table 5. Parameters of the best-fitting silicate emissivity spectra, H_2O ice data from Whittet et al. (1988), and optical depth and column-density limits for methanol and HMT. Numbers in brackets are exponents. Column densities are measured in molecules cm^{-2}.

		Silicate			H_2O		Methanol		HMT	
λ/μm		9.7			3.0		9.8		10.0	
Δλ/μm[a]		see below			0.23		0.36		0.20	
σ_{int}[b]/cm^2 μm mol^{-1}		1.1(-18)			1.9(-19)		1.7(-19)		5.0(-20)	
Source	Emissivity	Δλ /μm	τ_{sil}	N(sil)	τ	$N(H_2O)$	τ	$N(CH_3OH)$	τ	N(HMT)
Cyg OB2 no.12	μ Cephei	2.6	0.62	1.5(18)	<0.02[c]	<4.0(16)[c]	-	-	<0.0067	<2.7(16)
Taurus-Elias 13	Simpson Group 2	3.4	0.53	1.6(18)	0.65±0.06	7.8(17)	-	-	-	-
Taurus-Elias 16	Trapezium	3.3	0.81	2.4(18)	1.60	1.9(18)	<0.040	<8.3(16)	<0.058	<2.3(17)
Taurus-Elias 18	Trapezium	3.2	0.44	1.3(18)	0.80±0.06	9.6(17)	<0.026	<5.5(16)	<0.016	<6.5(16)

[a] Mean wavelength and FWHM of feature measured from laboratory spectra by Hudgins et al. (1993).
[b] Integrated cross-section of band: silicate, H_2O and methanol (Skinner et al. 1992); HMT (Bernstein et al. 1995).
[c] H_2O ice upper limits for Cyg OB2 no. 12 from *ISO* spectra by Whittet et al. (1997).

4.3 Laboratory silicates

Similar comparisons were made to the laboratory spectra of ground (crystalline) and condensed (amorphous) olivine and enstatite given by Stephens & Russell (1979), and to spectra of amorphous diopside, synthetic and natural olivines, a synthetic cosmic silicate and a natural serpentine given by Blanco et al. (1993). There are differences in the properties of the spectra produced by these two sets of amorphous silicates. The features produced by olivines peak near 9.8 μm, while there is a range of peak wavelengths for chain silicates. Also, the optical depth at the long-wavelength end of the band produced by Stephens & Russell's olivine condensate is three times that of the Blanco et al. olivines, effectively increasing the breadth of the feature. Apart from the case of Elias 13, which again does not discriminate between a variety of possible fits, the spectra of amorphous silicates presented by Blanco et al. are the best-fitting laboratory spectra. In all cases, the best Stephens & Russell fits – olivine condensate (Cyg OB2 no. 12), enstatite condensate (Elias 18) and ground enstatite (Elias 13 and 16) – were much inferior to those obtained with the Trapezium and μ Cephei emissivities; in two cases their amorphous condensate spectra gave worse fits than even the fine-structured spectrum of crystalline enstatite. There is a greater degree of uniformity in the interstellar spectra than in the lab specimens: the five spectra produced by Blanco et al. fit all the observations, except that of Elias 13, in the same order when sorted by increasing χ^2: diopside, synthetic olivine, synthetic cosmic silicate, serpentine and natural olivine.

4.4 Overview

In accordance with the conclusion of Whittet et al. (1988), the broad Trapezium emissivity best fits the molecular cloud silicate absorption, while the diffuse ISM is best matched by the narrower μ Cephei emissivity. Excluding the noisy spectrum of Elias 13, these two emissivities fit the observations better than Simpson's circumstellar emissivities, or the laboratory spectra of synthetic silicates and minerals. Using the best fits to fix the ratio of continuum to silicate feature opacity at 8 and 13 μm, we present in Fig. 2 the derived optical depth profiles for these lines of sight. The essential similarity of the features in Elias 16 and 18 suggests that the processing responsible for altering icy grain mantles in the latter source (Section 3.2) has had little effect on the silicate substrates. This contrasts with the finding of Hanner et al. (1994a) that the silicate *emission* feature in the embedded source Taurus-Elias 1 was poorly fitted by the Trapezium emissivity. Peak optical depths measured from our spectra produce the silicate column densities in these lines of sight, listed in Table 5.

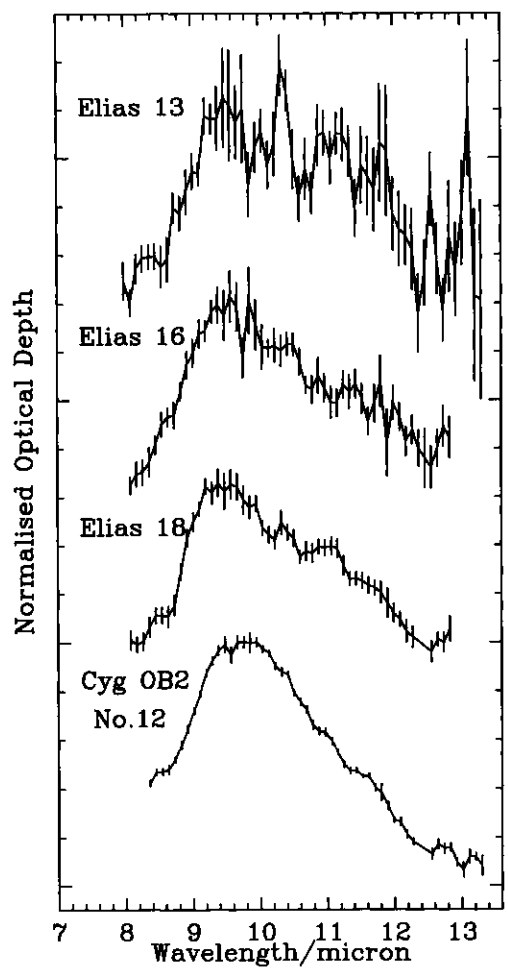

Figure 2. Derived intrinsic silicate features for the four lines of sight, with relative optical depth of the feature and the continuum fixed by the best-fitting emissivity given in Table 5.

© Royal Astronomical Society • Provided by the NASA Astrophysics Data System

1998MNRAS.298..131B

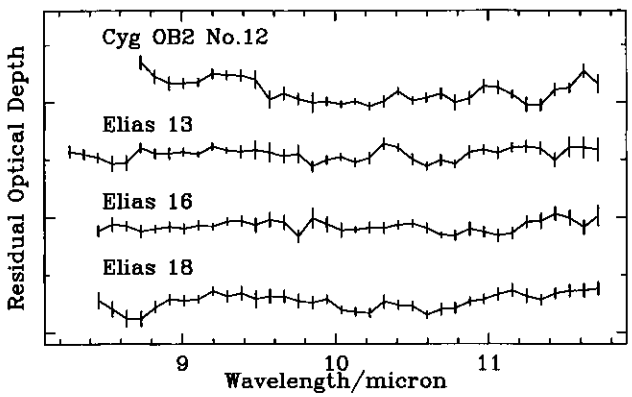

Figure 3. Limits on fine structure; all spectra are normalized with respect to their mean errors, and shifted in the y-axis for clarity.

On the short-wavelength wing, the feature is essentially independent of environment (Fig. 2): the greater breadth of the molecular cloud silicate feature is a product of the presence of *an extended long-wavelength wing*, most of which is attributable to an excess about 2 μm in width, centred at 11.5 μm. This wing is much weaker, or absent, in the spectrum of Cyg OB2 no. 12. The match between the molecular-cloud spectra and the Trapezium emissivity, which derives from dust well above the sublimation temperature of H_2O ice, suggests that this feature is not associated with volatile grain mantle material. It is unlikely to be associated with the libration band of solid H_2O, which peaks at 13–14 μm in typical ice: (Hudgins et al. 1993). If this feature represents the shifted peak characteristic of large grain sizes (Hanner et al. 1994b), grain growth up to the order of 1 μm occurs in the cloud medium, and is not associated exclusively with embedded sources.

4.5 Limits on fine structure

Laboratory studies of bulk crystalline silicates show spectral fine structure, which is smoothed out in amorphous materials of essentially the same composition (compare, for example, glassy and crystalline samples of bronzite; Dorschner et al. 1988). Although fine structure indicative of crystalline olivine is present in the silicate feature in comet Halley (e.g. Campins & Ryan 1989), the only evidence for the presence of a crystalline component in the interstellar 10-μm band to date derives from the *polarization* spectrum of GL 2591 (Aitken et al. 1988).

To place limits on fine structure in the interstellar spectra, each optical depth spectrum was divided by its best-fitting emissivity to remove the amorphous silicate feature. Time-varying telluric water, ozone, and poor atmospheric transmission (Cohen & Davies 1995) preclude the detection of weak structures outside the relatively clean part of the spectrum between 8.2 and 11.7 μm (cancellation of the atmospheric ozone feature was excellent during the observations). To compare the data between these limits, each spectrum was normalized with respect to its mean error (Fig. 3). There are clearly no *major* structures in common between the objects, even though Elias's objects are all obscured by the same molecular cloud complex. The only potentially reproducible feature is a $1–2\sigma$ bump at about 10.4 μm.

For a basic comparison with mineral spectra in terms of the presence or absence of fine structure, infrared silicate transmittance spectra were selected (mainly from Ferraro 1982) according to their occurrence in IDPs and meteorites, the cosmic abundances of elements (Anders & Grevesse 1989), the smoothness of their infrared spectra between 7.8 and 30 μm, and the simplicity of their chemical formulae. The relative heights of peaks in the optical depth spectra of crystalline minerals vary between publications (e.g. Dorschner, Friedemann & Gürtler 1978; Ferraro 1982; Dorschner et al. 1988; Blanco et al. 1992). The peaks take up characteristic wavelengths for a given crystalline mineral. Typical matrix shifts in laboratory spectra are small, corresponding to about two data points in our spectra. Only two types of silicate produce narrow structure at ~10.4 μm – the chain silicates such as diopside and bronzite (Ferraro 1982; Dorschner et al. 1988) and crystalline serpentine (Dorschner et al. 1978; Ferraro 1982; Blanco et al. 1992). Of these, only serpentine produces no structure of similar strength elsewhere in the 10-μm window. Whittet et al. (1997) found a weak absorption feature near 2.75 μm in their *ISO* spectrum of Cyg OB2 no. 12, which they attribute to the presence of hydrous, layer-lattice silicates such as serpentine, accounting for only a few per cent by mass of the silicate dust in the line of sight. If the 10.4-μm feature *does* represent a narrow band of such a silicate, then its optical depth is only about a few per cent of that of the main band; it is clearly a minor constituent of the dust population, which remains largely amorphous.

5 GRAIN MANTLES

5.1 H_2O ice

The widespread presence of water ice in the Taurus cloud has been well known for some time (e.g. Whittet et al. 1988), and the three Taurus objects presented here show relatively deep absorption in the 3-μm ice band. Smith, Sellgren & Brooke (1993) accounted for the observed 3-μm ice band profile in Taurus by invoking thick layers of amorphous H_2O. Because the available oxygen abundance precludes the presence of ice mantles this thick on *all* grains, they proposed the presence of two populations of grains – one mantled, one unmantled – with the latter outnumbering the former by a factor of 3×10^4. Scattering calculations by O'Donnell (1994) show that mantling silicate cores with amorphous ice raises the short-wavelength wing of the silicate absorption substantially if the mantle/core volume ratio approaches 3 (a criterion easily fulfilled by the thickly coated grains invoked by Smith et al.). However, the 8-μm region of the spectrum of Elias 16 shows no evidence for excess optical depth by comparison with Elias 13, although the former source has two times deeper H_2O ice absorption at 3 μm. If the interpretation by Smith et al. is correct, then the coated grains are not uniquely identified with the silicates.

H_2O ice produces a broad 'libration' band between 10 and 20 μm. The absorption strength of this band ($\sigma_{\rm int}$ is 6×10^{-19} cm^2 μm molecule^{-1}, while that of the 3-μm O–H stretch 'ice band' is 2×10^{-19} in the same units. The bands are 4.5–5.3 and 0.33 μm wide respectively (the former is dependent on mantle composition, but the latter is an observational average of many objects, and should be accurate to 10 per cent). Assuming that the same number of ice molecules is sampled by both bands, $\tau \Delta\lambda/\sigma$ = constant and $\tau_{\rm lib} \approx 0.2\tau_{3.1}$. Data from Whittet et al. (1988) for the 3.1-μm band then predict libration band optical depths of 0.13, 0.32 and 0.16 for Elias 13, 16 and 18 respectively. If libration features with those optical depths are present and centred around 13 μm, they might contribute to the long-wavelength wing of the 'silicate' feature. However, the three Taurus sources have essentially the same profile irrespective of 3-μm optical depth. High optical depth in the ice band thus reflects larger column densities of all grain material, rather than thicker grain mantles.

© Royal Astronomical Society • Provided by the NASA Astrophysics Data System

1998MNRAS.298..131B

5.2 Other mantle components

Methanol is a key ingredient for photolysis, and its abundance in simple unprocessed ices is therefore an important parameter. For example, Bernstein et al. (1995) use a starting mixture in which the methanol abundance is 50 per cent that of water ice. Measurements of the 3.54-μm methanol band indicate abundances much lower than this in quiescent cloud ices (e.g. Chiar et al. 1996), but such observations are difficult and constraints based on other features are useful. Skinner et al. (1992) pointed out the existence of a methanol band at 9.8 μm, and the spectra presented here have sufficiently high signal-to-noise ratios at that wavelength to permit sensitive measurements of the methanol abundance in the Taurus cloud. Fitting the narrow methanol band using a third-degree polynomial continuum to remove wider scale variations (which in fact serve to decrease the inferred upper-limit methanol abundance) produces optical depth and column-density limits (68 per cent confidence) as given in Table 5. In all cases, the best-fitting methanol feature (represented by a Gaussian) is consistent with zero optical depth. The upper-limit abundances in Elias 16 and 18 are ~5 per cent that of H_2O (Table 5). These results independently confirm the low limits determined by Chiar et al. (1996). The spectrum of Elias 13 is too noisy to produce a useful limit.

Laboratory photolysis of simple ices, followed by warming up of the residue, produces a nitrogen-bearing substance in which the cage molecule hexamethylenetetramine (HMT) has been identified (Bernstein et al. 1995). The amount of this substance produced depends on the abundance of ammonia and methanol in the initial ice. Sharp spectral features are produced across the mid-infrared by HMT: one of these falls within the range of the spectra presented here. Although we do not expect it to be present in the icy mantles typical of the Taurus cloud, it is of interest to place a limit on the abundance of this substance in the diffuse ISM and in the heated region close to Elias 18. Given that the lifetime of HMT in the diffuse ISM may be short, the spectrum of Elias 18 offers the best prospect of detecting HMT in the current data set. The maximum (68 per cent confidence) optical depth allowed by our spectra in the 9.95-μm HMT band was determined and combined with the band absorption strength given by Bernstein et al. The resulting column densities are tabulated in Table 5. The 1σ upper-limit HMT abundances in Elias 18 and Cyg OB2 no. 12 are a few per cent of the corresponding silicate column densities.

6 SUMMARY

Silicate absorptions in the diffuse ISM (Cyg OB2 no. 12), a quiescent molecular cloud (Taurus-Elias 13 and 16) and an embedded YSO (Taurus-Elias 18) have been presented and compared with the emissivity spectra of astronomical, synthetic and mineral silicates. The breadth of the silicate feature in dark clouds results from the presence of well-defined excess absorption in the long-wavelength wing of the band. This excess is weak in the diffuse ISM, accounting for the known narrowness of the feature in the latter environment. By contrast, the short-wavelength side of the feature is almost independent of environment and the presence or absence of mantles.

The emissivity of heated (250 K) dust in the Trapezium cluster fits the spectrum of quiescent molecular-cloud absorption better than any known circumstellar emissivity, whereas a circumstellar (μ Cephei) emissivity provides the best fit to the spectrum of the diffuse ISM. The Trapezium and μ Cephei fits to dense and diffuse regions, respectively, are better than those based on any other spectra with which a comparison was made. Although the difference between recently formed dust and that in molecular clouds is confirmed by these high-quality spectra, this difference is small compared to those between the astronomical spectra and the range of laboratory silicates studied.

There is no evidence of significant fine structure in the stable region of high signal-to-noise ratio between 8.2 and 11.7 μm. A possible common feature at 10.4 μm, of order a few per cent of the optical depth of the broad 9.7-μm band, is most plausibly linked to the layer-lattice silicate serpentine, for which there is also evidence in *ISO* spectra of the 2.7–3.0 μm region.

Upper limits on the constituents of grain mantles were obtained. There is no evidence for the 13-μm absorption attributable to H_2O ice in the data. The methanol abundance in the Taurus molecular cloud sources, obtained from the band at 9.8 μm, is at most a few per cent of that of H_2O along the same line of sight. The abundance of HMT in the diffuse ISM is low and not greater than 2 per cent of the silicate abundance in the same line of sight.

ACKNOWLEDGMENTS

This work was based on data obtained with the UK Infrared Telescope, Mauna Kea Observatory, Hawaii, reduced and analysed using Starlink facilities at the University of Central Lancashire.

We thank the staff of UKIRT for an excellent observing run, and the anonymous referee for a critical reading of this paper, including comments regarding the stellar wind of Cyg OB2 no. 12. AJA is partly funded by the University of Central Lancashire, and partly by the UK Starlink project; at the time of writing, Janet Bowey held a University of Central Lancashire research studentship.

REFERENCES

Abbott D. C., Telesco C. M., Wolff S. C., 1984, ApJ, 279, 235
Adamson A. J., Whittet D. C. B., Duley W. W., 1990, MNRAS, 243, 400
Aitken D. K., Roche P. F., Smith C.H., Hough J. H., 1988, MNRAS, 230, 629
Anders E., Grevesse N., 1989, Geochim. Cosmochim. Acta, 53, 197
Bernstein M. P., Sandford S. A., Allamandola L. J., Chang S., Scharberg M. A., 1995, ApJ, 454, 327
Blanco A., Orofino V., Martino M., Fonti S., Stephens J. R., 1992, Il Nuovo Cimento, 15C, No. 6, 1091
Blanco A., Fonti S., Martino M., Bussoletti E., Mennella V., Colangeli L., Stephens J. R., 1993, in Kwok S., ed., ASP Conf. Ser. Vol. 41, Astronomical Infrared Spectroscopy: Future Observational Directions. Astron. Soc. Pac., San Francisco, p. 267
Bregman J. D., Campins H., Witteborn F. C., Wooden D.H., Rank D. M., Allamandola L. J., Cohen M., Tielens A. G. G. M., 1987, A&A, 187, 616
Campins H., Ryan E. V., 1989, ApJ, 341, 1059
Chiar J. E., Adamson A. J., Kerr T. H., Whittet D. C. B., 1995, ApJ, 455, 234
Chiar J. E., Adamson A. J., Whittet D. C. B., 1996, ApJ, 472, 665
Cohen M., Davies J. K., 1995, MNRAS, 276, 715
Day K. L., Donn B. D., 1978, ApJ, 222, L45
Dorschner J., Friedemann C., Gürtler J., 1978, Astron. Nachr., 299, 269
Dorschner J., Friedemann C., Gürtler J., Henning Th., 1988, in Bussoletti E. et al., eds, in Experiments on Cosmic Dust Analogues. p. 209
Elias J. H., 1978, ApJ, 224, 857
Ferraro J. R., 1982, Sadtler Research Laboratories
Forrest W. J., Gillett F. C., Stein W. A., 1975, ApJ, 195, 423
Gezari D. Y., Schmitz M., Pitts P. S., Mead J. M., 1993, NASA Ref. Publ. 1294
Gürtler J., Dorschner J., Mutschke H., Henning Th., 1993, in ASP Conf. Ser. Vol. 41, Astronomical Infrared Spectroscopy: Future Observational Directions. Astron. Soc. Pac., San Francisco, p. 273
Hanner M. S., Brooke T. Y., Tokunaga A. T., 1994a, ApJ, 433, L97

© Royal Astronomical Society • Provided by the NASA Astrophysics Data System

1998MNRAS.298..131B

Hanner M. S., Lynch D. K., Russell R. W., 1994b, ApJ, 425, 274
Hanner M. S., Brooke T. Y., Tokunaga A. T., 1995, ApJ, 438, 250
Hudgins D. M., Sandford S. A., Allamandola L. J., Tielens A. G. G. M., 1993, ApJS, 86, 713
Humphreys R. M., 1978, ApJS, 38, 309
Jäger C., Mutschke H., Begemann B., Dorschner J., Henning Th., 1994, A&A, 292, 641
Martin P. G., Whittet D. C. B., 1990, ApJ, 357, 113
O'Donnell J. E., 1994, ApJ, 437, 262
Persi P., Ferrari-Toniolo M., 1982, A&A, 111, L7
Press W. H., Teukolsky S. A., Vetterling W. T., Flannery B. P., 1992, Numerical Recipes. Cambridge Univ. Press, Cambridge
Rieke G. H., 1974, ApJ, 193, L81
Roche P. F., Aitken D. K., 1984, MNRAS 208, 481
Roche P. F., Aitken D. K., 1985, MNRAS, 215, 425
Russell R. W., Soifer B. T., Forrest W. J., 1975, ApJ, 198, L41
Sandford S. A., 1989, in Allamandola L. J., Tielens A. G. G. M., eds, Proc. IAU Symp. 135, Interstellar Dust. Kluwer, Dordrecht, p. 403
Sandford S. A., Walker R. M., 1985, ApJ, 291, 838
Simpson J. P., 1991, ApJ, 368, 570
Skinner C. J., Tielens A. G. G. M., Barlow M. J., Justtanont K., 1992, ApJ, 399, L79
Smith R. G., Sellgren K., Brooke T. Y., 1993, MNRAS, 263, 749
Stephens J. R., Russell R. W., 1979, ApJ, 228, 780
Tamura M., Sato S., 1989, AJ, 98, 1368
Tegler S. C., Weintraub D. A., Rettig T. W., Pendleton Y. J., Whittet D. C. B., Kulesa C. A., 1995, ApJ, 439, 279
Whittet D. C. B., Bode M. F., Longmore A. J., Adamson A. J., McFadzean A. D., Aitken D. K., Roche P. F., 1988, MNRAS, 233, 321
Whittet D. C. B. et al., 1997, ApJ, 490, 729

© Royal Astronomical Society • Provided by the NASA Astrophysics Data System